Effective drag on spheres immersed in a fluidized bed at minimum fluidization—Influence of bulk solids properties

Received: 8 December 2021 | Revised: 26 March 2022 | Accepted: 29 March 2022

DOI: 10.1002/cjce.24575

SPECIAL ISSUE ARTICLE

THE CANADIAN JOURNAL OF CHEMICAL ENGINEERING

Effective drag on spheres immersed in a fluidized bed at minimum fluidization—Influence of bulk solids properties

Diana Carolina Guío-Pérez[1] | **Anna Köhler**[1] | **Anna Prati**[2] | **David Pallarès**[1] | **Filip Johnsson**[1]

[1]Department of Space, Earth and Environment, Division of Energy Technology, Chalmers University of Technology, Gothenburg, Sweden

[2]Faculty of Science and Technology, Free University of Bozen-Bolzano, Bolzano, Italy

Correspondence
Diana Carolina Guío-Pérez, Department of Space, Earth and Environment, Division of Energy Technology, Chalmers University of Technology, Hörsalvägen 7B, SE-412 96, Göteborg, 41296, Sweden.
Email: carolina.guioperez@chalmers.se

Funding information
Energy Area of Advance at Chalmers University of Technology; Swedish Energy Agency through the Swedish Gasification Center (SFC), Grant/Award Number: P-38347-2

Abstract

The aims of this work are to elucidate the effects that bulk solids properties have on the effective drag experienced by large spheres immersed in an emulsion of group-B solids under minimum fluidization conditions and to analyze the ways in which the different suspensions react towards different applied shear rates. To investigate this, magnetic particle tracking was applied to resolve the trajectory of falling-sphere measurements in which the size, density, and sphericity of the bulk solids were varied as well as the size and density of the spherical tracers. The resulting experimental scope included both rising and sinking tracers as well as full segregation and in-bed stagnation of the tracers. The set-up provided highly resolved tracer trajectories, from which the drag experienced by the sphere can be calculated. For sinking tracers, the results showed that an increase in bulk solids size, angularity, and density reduced the terminal velocity of the sphere. This effect correlated well with the bed expansion and Hausner ratio, indicating that a reduced void space among the bulk solids is the main reason for the increase in motion resistance. At lower shear rates, namely, during the de-acceleration towards the stagnant state, beds of larger, more angular, or denser bulk solids yield lower levels of shear stress. The angle of repose of the bulk solids correlated with the rate at which the emulsion thins with increasing shear rate. For rising tracers, shear stress did not show any significant dependency on the properties of the bulk solids.

KEYWORDS

drag force, effective viscosity, fluidized bed, gas–solids flow, magnetic-particle-tracking

1 | INTRODUCTION

Gas–solids fluidized bed (FB) units, which are widely used in reactive and thermal processes, involve as a key aspect the transfer of mass, momentum, and heat between the fluidized emulsion of gas and bulk solids and the reactive particles immersed in the emulsion. The efficiency of the overall fluidized-bed process depends to

a large extent on the possibility to control the mixing of the immersed particles (which are typically larger and of different density than the bulk solids) through momentum transfer with the bed. This is the case of FB applications in thermal conversion of solid fuels (e.g., combustion, gasification, and pyrolysis), calcination of metal particles, and the separation of larger solids in segregators.[1] Yet, observations from operating FB units (particularly under bubbling conditions) indicate maldistribution of the immersed particles,[2] and it is not obvious how to reduce such inhomogeneities through design improvements or, in existing plants, by means of process control and/or feedstock pre-treatment.

Despite the many industrial applications that involve the presence of larger particles immersed in a FB of smaller particles (e.g., solid fuel conversion, drying, coating, and separation), there is a lack of understanding of the momentum exchange that occurs between these large particles and the solids suspension. This knowledge gap hinders the establishment of fully reliable descriptions of the mixing. Thus, much of the design and scale-up of such FB processes is empirical. As the basis for mathematical modelling of fluid-dynamic phenomena in FB units, there is a need to characterize the rheologic properties of the bed in terms of the momentum transfer with immersed larger particles through an effective drag force. Professor J. R. Grace was early to discuss the analogy between liquids and dense FBs and proposed assigning a viscosity to the FB.[3] He called for the need to measure the shear stresses developed in FBs and their relationship with the movement of bubbles and the stability of the bed. The shear stress studies existing at that moment and summarized by Grace in his early paper were mainly based on theoretical deductions and observation of the shapes and behaviour of the bubbles. With the recent development of time-resolved measurement techniques, it should be possible to get further experimental insights into the shear stresses, and thereby the effective viscosity in the dense region of FBs, which remains still a relatively unexplored aspect of fluidization.

The well-established two-phase flow theory for gas–solids fluidization proposes a division of the gas flow into two parts: the flow maintaining the dense phase in-between bubbles under minimum fluidization and the visible bubble flow, that is, the flow in excess of minimum fluidization.[4] However, at high fluidization velocities applying to group B and D solids (for which the dense phase can be assumed to remain at minimum fluidization conditions), a throughflow of gas through the bubbles has been observed,[5] which is required in order to close the mass balance while not overestimating the bed expansion due to the bubbles. Thus, minimum fluidization conditions are of special interest and remain the basis of studies of many fluid dynamic phenomena in bubbling FBs, which can be combined with studies on the macroscopic movement of the gas–solids emulsion[6] to offer a full description of the mixing of solids immersed in a FB. Several authors have attempted to derive the drag on immersed larger objects imposed by gas–solids emulsions under minimum fluidization (yielding particle volume fractions typically around 0.6).[3,7–12] These investigations have offered a theoretical analysis of the flow of such emulsions around immersed particles and shown that:

- While the assumption that a gas FB (as a homogeneous emulsion) exhibits Newtonian behaviour (invariable proportionality between the shear stress and the applied shear rate) has been inferred[3] or assumed[13,14] in some studies, more precise measurements have challenged this assumption and proposed alternative models, which indicate both a plastic behaviour (varying rate of the change in shear stress with shear rate) and a yield stress (non-zero shear stress at zero shear rate).[15–18]
- Immersed-body-type studies are often used in the analysis of fluids. Although they provide reliable information about flow parameters (particularly at near-zero shear rates), it should be noted that the movement of a non-Newtonian fluid around a body is non-viscometric (the shear stress and shear rate are not uniform), which means that the results can only be directly related to local phenomena.[7] The results from falling-sphere measurements are complementary (and not necessarily comparable) to those obtained using methods in which the fluid (e.g., capillarity measurements) or the emulsion (e.g., rotating cylinders) is not perturbed.[18,19]

In addition, extensive research has been carried out on other multiphase systems. Liquid-solids FBs are often treated as Newtonian fluids; Gibilaro et al.[13] have summarized the major developments in such systems. However, several groups[20–22] have reported complex effects of the suspension rheology that, to some extent, can be seen as analogous to the emulsion of gas–solids FBs. Investigation of drilling slurries and polymer emulsions not only have increased our understanding of the time-dependence of viscosity and the presence of the yield stress in liquid–solids suspensions but also have demonstrated the impacts of particle concentration, size, and shape on the rheology of the emulsion. Most of these effects have been compiled in key publications, such as those of Kamal and Mutel,[23] Coussot,[24] and Willenbacher and Georgieva.[25] The field of granular flows has similarly contributed to a better understanding of the

bulk solids dynamics in dense suspensions[26–28] and their interactions with immersed bodies. Despite this accumulated knowledge, the study of the flow properties of gas–solids FBs is still incipient, with much remaining to be discovered.

A recurrent challenge in studies of gas–solids flows is the lack of experimental techniques that are sufficiently accurate to capture the key flow features occurring at shorter lengths and time scales. As a consequence, these investigations are typically limited to using general assumptions, such as Stokes' law,[14,29] and complementing the low resolution of experimental data with modelling.[30,31] Fortunately, magnetic particle tracking[32] has recently made it possible to track an immersed particle accurately, and it has been proven to be a consistent tool for studying the effective drag on a sphere immersed in a gas–solids emulsion at minimum fluidization.[33]

The above-cited study[33] has revealed the non-Newtonian character of the emulsion when acting on immersed spheres and provided evidence of viscoplastic characteristics at low shear rates, which have found their best fit in the original rheology model of Herschel–Bulkley.[34] In similarity to other viscoplastic models (described in, e.g., work by Chhabra[7] and Coussot[24]), the Herschel–Bulkley model considers a yield stress (shear stress at zero shear rate) and a non-linear increase in the shear stress as the shear rate grows, characterized by the consistency term (analogous to viscosity) and the flow index (a measure of shear-thinning). Further, for high values of the shear rate, measurements by Köhler et al.[33] have also shown a decrease in the shear stress down to the value of the yield stress, which suggests eventual changes in the distribution of solids in the emulsion (e.g., local increase in concentration).

With a better understanding of the general characteristics of the drag exerted on immersed spherical particles by the gas–solids emulsion at minimum fluidization, questions have arisen concerning the impacts of the properties of the bulk solids. For other types of suspensions, such as slurries and colloids,[23–25] the solids properties are reported to influence the capacity of the solids to rearrange in the suspension and thereby on the characteristics of the momentum exchange between the suspension and the moving object. In the case of gas–solids fluidization, bulk solids are primarily characterized by their size, density, and sphericity.

The aim of the present work is to extend current understanding of the momentum exchange between a gas–solids emulsion at minimum fluidization and an immersed sphere that is larger than the bulk solids. For this, the present work uses the experimental methodology developed by Köhler et al.[33] to gain insights into how the properties (size, sphericity, and density) of the bulk solids impact the effective drag force established between a gas–solids emulsion at a minimum fluidization and a larger immersed particle. Particular attention is paid to terminal conditions, namely, when the immersed sphere reaches a constant non-zero velocity or stagnates within the emulsion. For the analysis, we combine measurements with magnetic particle tracking (since such experiments give high levels of accuracy and resolution) with force balances that include expressions for the drag force. The scope of this study is limited to spherical tracers immersed in a gas–solids emulsion at minimum fluidization velocity (air is used as gas and Geldart group B[35] solids as bulk material, which is typically used in the thermal conversion of solid fuels).

2 | THEORY

The original falling-sphere method for estimating viscosity in viscous fluids involves different spherical tracers with defined sizes and densities being released in a standpipe filled with the fluid of interest. In a viscous fluid that is homogeneous and at rest, the free movement of a sphere released inside is governed by vertical forces, mainly gravity and drag.[7,24] Therefore, only the analysis of vertical movements is relevant. The time required for the sphere to sink through the standing fluid is measured based on the assumption that the sphere will reach a terminal velocity, namely, a constant velocity, during its movement inside the fluid. In this way, the effects of a non-Newtonian rheology, such as velocity variations (and possible stagnation) of the sphere, are not resolved by the method. Thus, being able to measure the instant velocity of the sphere throughout its trajectory allows one to solve the force balance in the vertical direction for every position of the sphere and to extract detailed information about the effective drag acting on the particle at different velocities (corresponding to different shear rates). By modifying the size and density of the sphere, the shear rate can be varied and the dependency on the size ratio of the bulk solids to the sphere can be explored.

Under minimum fluidization conditions, the homogeneous concentration of bulk solids enables an analogy to be drawn between the gas–solids emulsion and a liquid. Thus, the force balance for a sphere moving in the z (vertical) direction can be written:

$$m_p \frac{du_z}{dt} = \sum F = F_G + F_B + F_D + F_V \qquad (1)$$

where m_p and u_z are the mass and the vertical velocity of the sphere, respectively, and t is time. F_G is the gravity term, F_B is the buoyancy term, F_D is the drag term, and

F_V is the virtual mass term.[36] Wall effects are expected to play a minor role for Reynolds numbers up to ~100 as applied in this work[37] and are, therefore, neglected in this analysis. Thus, with the assumption of the gas–solids emulsion at minimum fluidization (for which the gas phase drag and the virtual mass force have been found to be 3–4 orders of magnitude smaller than those of the other forces),[33] the force balance in Equation (1) yields:

$$\frac{\pi}{6}D_p^3\rho_p\frac{du_z}{dt}=\frac{\pi}{6}D_p^3\left(\rho_p-\rho_{em}\right)g+\frac{\pi}{8}D_p^2C_D\rho_{em}|u_{em}-u_z|^2 \tag{2}$$

where D_p and ρ_p are the diameter and density of the sphere, correspondingly. ρ_{em} corresponds to the density of the emulsion, g is the gravitational acceleration, C_D is the drag coefficient, and u_{em} is the velocity of the gas–solid emulsion resulting from the net vertical flow of bulk solids induced by the movement of the tracer. Thus, since the bed surface remains constant while the tracer is immersed into the gas–solids emulsion, an ascending tracer implies by continuity that the gas–solids emulsion moves downwards, and vice versa. Using the continuity equation, the velocity at any given time of the bulk solids in the emulsion surrounding the tracer can be calculated as:

$$u_{em}=-\frac{D_p^2}{\left(D_b^2-D_p^2\right)}u_z=-\lambda u_z \tag{3}$$

where D_p is the diameter of the bed container. This velocity is accounted for in the calculations, although the displacement of the emulsion caused by the immersion of the tracer particle has been found to have a minor impact.[33] The density of the emulsion can be determined based on the mass of bed material m_b, and the volume occupied by the bed at minimum fluidization, as shown in Equation (4):

$$\rho_{em}=\varepsilon_{mf}\rho_g+(1-\varepsilon_{mf})\rho_s\approx\frac{m_b}{A_bL_{mf}} \tag{4}$$

where ε_{mf} is the voidage of the bed at minimum fluidization, ρ_g is the density of the gas, ρ_s is the density of the bed solids, A_b is the cross-sectional area of the container, and L_{mf} is the height of the bed under minimum fluidization conditions. With these considerations and given a trajectory of the tracer, the drag coefficient can be solved from Equations (2)–(4), and the shear stress can be calculated from Equation (5). Note that the assumption of negligible emulsion velocity (λ=0) considerably simplifies the expression. Given the use of different sphere sizes (which allow the achievement of different shear rates), direct comparison of the drag force across different experiments is not suitable for analysis. Nevertheless, calculating the shear stress offers a way to normalize the results with respect to the geometry of the immersed body. In addition, using the surface area of the immersed sphere (thus, the emulsion-tracer contact area) in the calculation of the shear stress gives the obtained stress values relevance for both the tracer and the emulsion.

$$\tau=\frac{F_D}{A_s}=\frac{1}{8}C_D\rho_{em}(1-\lambda)^2u_z^2=\frac{1}{6}D_p\left(g\left(\rho_{em}-\rho_p\right)+\frac{du_z}{dt}\rho_p\right) \tag{5}$$

For the evaluation of the shear rate, the definition of characteristic shear rate suggested by Chhabra[7] is used, that is, u_{rel}/D_p, where u_{rel} is the relative velocity of the tracer to the bulk solids velocity. This parameter is often used to analyze falling particle experiments and normalizes the slip velocity with the characteristic length of the momentum transfer (here, the size of the immersed particle, which relates to the thickness of the fluid-dynamic boundary layer). In this way, the precise measurement of the velocity of the tracer while it moves freely inside the fluid (here, the gas–solids emulsion) allows one to calculate both the shear rate and shear stress at every position, thereby revealing details of their relationship.

For non-Newtonian fluids that exhibit a yield stress, a commonly used strategy to study the relationship between stress forces and gravitational forces is to normalize the shear stress according to the tracer buoyancy, reading:

$$Y=\frac{\tau}{gD_p\left(\rho_{em}-\rho_p\right)} \tag{6}$$

In this way, the dependency on the sphere's properties is removed and the net ratio of stress to gravitational forces can be analyzed. Consequently, the yield gravity parameter Y_0, namely, the normalized shear stress at zero shear rate, can be defined. This parameter is often used to discuss the static equilibrium of spheres in viscoplastic media.[7] Scrutiny of Equation (5) reveals that the normalized shear stress at equilibrium equals to $\frac{1}{6}$; thus, a normalized shear stress fluctuating around this value indicates a prevalence of the yield stress, while values above and below $\frac{1}{6}$ indicate dominant stress and net gravitational effects, respectively.

The effective viscosity is defined as the ratio of the average shear stress over the surface area of the object to the shear rate:

TABLE 1 Selected bulk bed materials and their principal physical properties

			Glass beads 250–300	Glass beads 150–180	Glass beads 125–150	Bronze 75–125	Sand 125–150	Glass beads 75–125	Alumina 75–125	Sand 75–125
Bulk solids properties	Particle size	μm	250–300	150–180	125–150	75–125	125–150	75–125	75–125	75–125
	Density	kg/m^3	2486	2486	2486	8471	2655	2486	1540	2655
	Sphericity	-	1	1	1	1	0.75	1	0.85	0.75
	Angle of repose	°	25.98	26.48	27.40	23.88	35.35	29.51	29.22	36.07
Bed properties	Bulk density	kg/m^3	1436	1448	1457	5149	1387	1438	925	1372
	Bed voidage at rest	-	0.285	0.428	0.428	0.389	0.479	0.434	0.419	0.479
	Bulk density at mf	kg/m^3	1407	1345	1324	5144	1346	1346	847	1349
	Bed voidage at mf	-	0.434	0.459	0.467	0.393	0.493	0.459	0.450	0.492
	u_{mf}	m/s	0.0604	0.0170	0.0123	0.0257	0.0170	0.0075	0.0045	0.0128
	Tapped bulk density	kg/m^3	1561	1565	1578	5487	1591	1548	1011	1579
	Hausner ratio	-	1.087	1.080	1.083	1.065	1.148	1.077	1.092	1.151
Variation	Size		*x*	*x*	*x*	-	-	*x*	-	-
	Density		-	-	-	*x*	-	*x*	*x*	-
	Sphericity		-	-	*x*	-	*x*	*x*	-	*x*

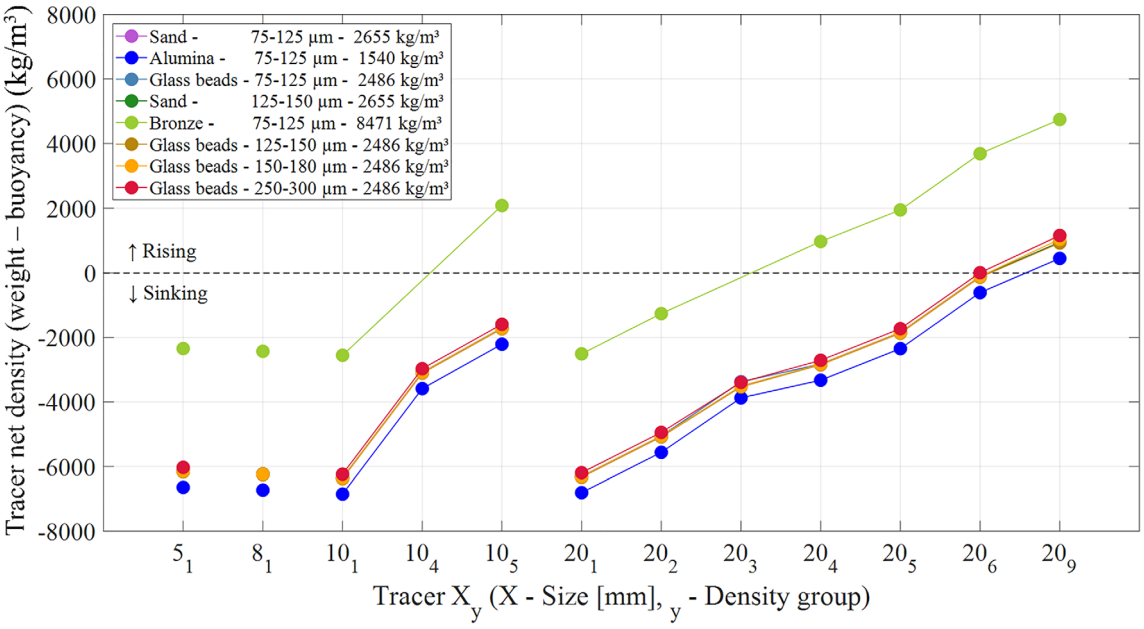

FIGURE 1 Spherical tracers used in the present study, displayed with their net densities in the different beds at minimum fluidization. The tracer names indicate their diameters in mm. Neutral buoyancy is indicated by a dashed line.

$$\tau = \mu_{\text{eff}}\dot{\gamma} \tag{7}$$

This relation can take different forms that define the rheologic behaviour of the fluid (here, a gas–solids FB under minimum fluidization), with the simplest being Newtonian fluids for which the viscosity is constant. However, for complex fluids, there is a dependency of the variation in shear stress on the shear rate, which has been described by different models (summarized in the study by Chhabra[7]). One of these models is the Herschel–Bulkley model, expressed by Equations (8) and (9), which has been shown to correctly describe a gas–solid emulsion at low shear rates[33]:

$$\tau = \tau_0^H + k\dot{\gamma}^n \quad \text{for } \tau > \tau_0^H \tag{8}$$

$$\dot{\gamma} = 0 \quad \text{for } \tau < \tau_0^H \tag{9}$$

where k is the consistency index, which gives an indication of the resistance of the fluid to flow; n is the flow-index, which gives an indication of how fast the resistance to flow changes with the shear rate; and τ_0 is the so-called 'yield stress', the initial stress that must be exceeded for the fluid to flow. For $n = 1$ and $\tau_0 = 0$, the fluid is Newtonian, while shear-thinning fluids ($n < 1$) that exhibit a yield stress ($\tau_0 > 0$) are termed 'viscoplastics'. A recent study[33] has revealed that the drag of a gas–solids emulsion on immersed larger spheres at shear rates <5 s^{-1} adopt viscoplastic behaviour and that can be ably described by Equations (8) and (9) with the fitting $Y_0 = \frac{\tau_0}{gD_p(\rho_{em}-\rho_p)} = 0.167$, $k_0 = 0.032$, and $n_0 = 0.501$.

3 | METHODOLOGY

3.1 | Characteristics of bulk particles and tracer spheres

Table 1 presents the properties of the bulk solids used in this work. A bed of each of these materials, subjected to minimum fluidization was used to perform a set of falling sphere experiments, in which every time a single magnetic tracer sphere was tracked by magnetic tracking. A systematic selection of bulk solids within the Geldart group B solids[35] was carried out by varying the particle size, density, and sphericity so as to analyze the resulting drag on the spheres with dependency on these properties. Sphericity of the bulk solids was estimated as the square of the circularity, which was determined by image analysis on microscopic pictures of the different bed materials. As bulk solids, the bed materials were characterized with respect to: the angle of repose (i.e., the steepest angle of descent relative to the horizontal plane to which the solids can be piled without slumping); bulk density; tapped bulk density (bulk density obtained by mechanically tapping the sample until no further volume change is observed, a property that reports on the degree of compression of the material when vigorously tapped)[38]; and the bed properties under minimum fluidization (expanded voidage and superficial gas velocity). The angle of repose is an indicator of the internal friction and flowability of the particulate material, while the other properties provide information about the void space in the emulsion. These properties are used later in the analysis of the results. The sets of beds used for each of the comparisons (particle size, density, and sphericity) are indicated in the lower part of the table ('variation'). Solids samples are prepared by sieving, thus the particle size values provided in Table 1 correspond to minimum and maximum sizes. The particle size distributions used are intentionally selected to be narrow to facilitate a stable state of minimum fluidization over the whole gas–solids suspension, which is especially challenging for group B solids.

To apply a wide range of shear rates, this work used 12 spherical tracers (falling sphere) of different sizes and densities. These consisted of magnetic material, so as to allow the following of the tracer by means of a magnetic tracking system. The tracers are presented in Figure 1, together with their sizes and density. Since the density of the solids suspension depends on the properties of the bulk solids, the same spherical tracer exhibits a different

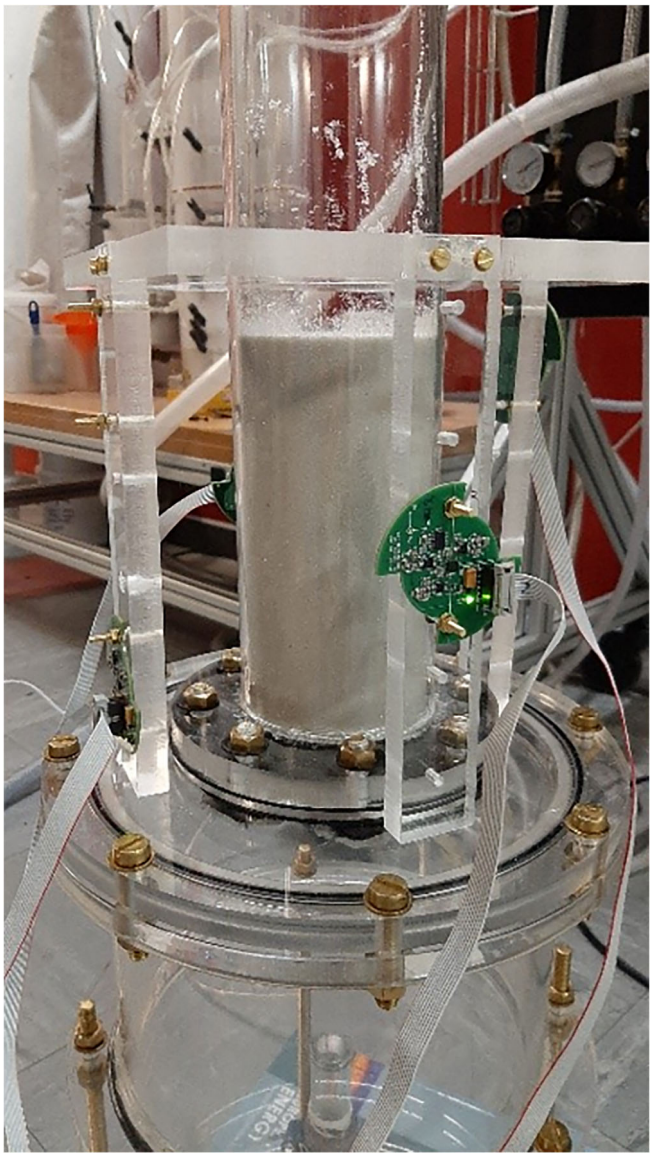

FIGURE 2 Experimental setup, depicting the fluidized bed and magnetic tracking system.

net buoyant density, and these values are differentiated on the plot by the use of different colours. The neutral buoyant density is indicated with a dashed line, indicating that tracer points lying below this line are expected to sink in the bed, while those above the line are expected to rise. It should be noted that although tracer 20_6 was slightly negatively buoyant in most of the beds, it did not sink in those beds but remained on the bed surface as a consequence of the yield stress.

3.2 | Experimental setup and procedure

The selected bulk solids were fluidized with pressurized air at room temperature under atmospheric pressure in a tube (with an inner diameter of 0.074 m). The unit was equipped with a high-resolution magnetic tracking system[39] that uses five sensors, each consisting of three anisotropic magneto resistance (AMR) sensors, as depicted in Figure 2. This system was used to measure

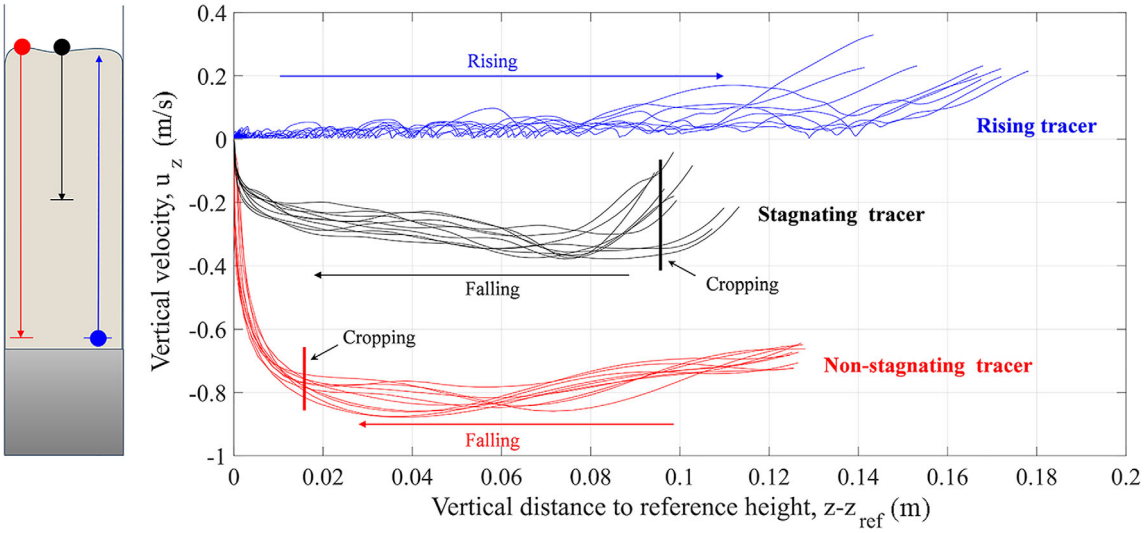

FIGURE 3 Examples of velocity profiles of the three behaviours identified from experiments plotted against the vertical location relative to a reference height (the starting point of the tracer, the stagnation height, or close to the bottom distributor, respectively): rising tracer, (sinking and) stagnating tracer, and (sinking and) non-stagnating tracer. The direction of the trajectory is indicated with arrows. Data cropping for the sinking tracers are indicated.

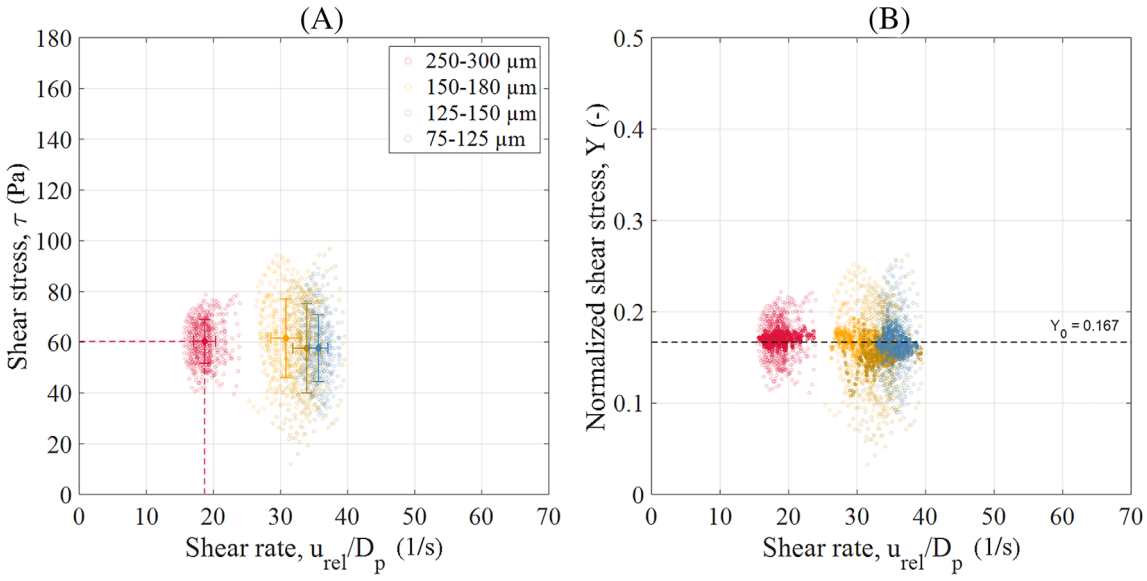

FIGURE 4 Rheograms corresponding to a tracer (here, $T20_5$) during a non-stagnating trajectory in different bulk materials (here, glass beads of different mean sizes). (A) Absolute variables. The centre of mass (average value) is indicated with the ♦ symbol and dashed lines. (B) Normalized variables. The normalized yield gravity parameter is indicated with a dashed line.

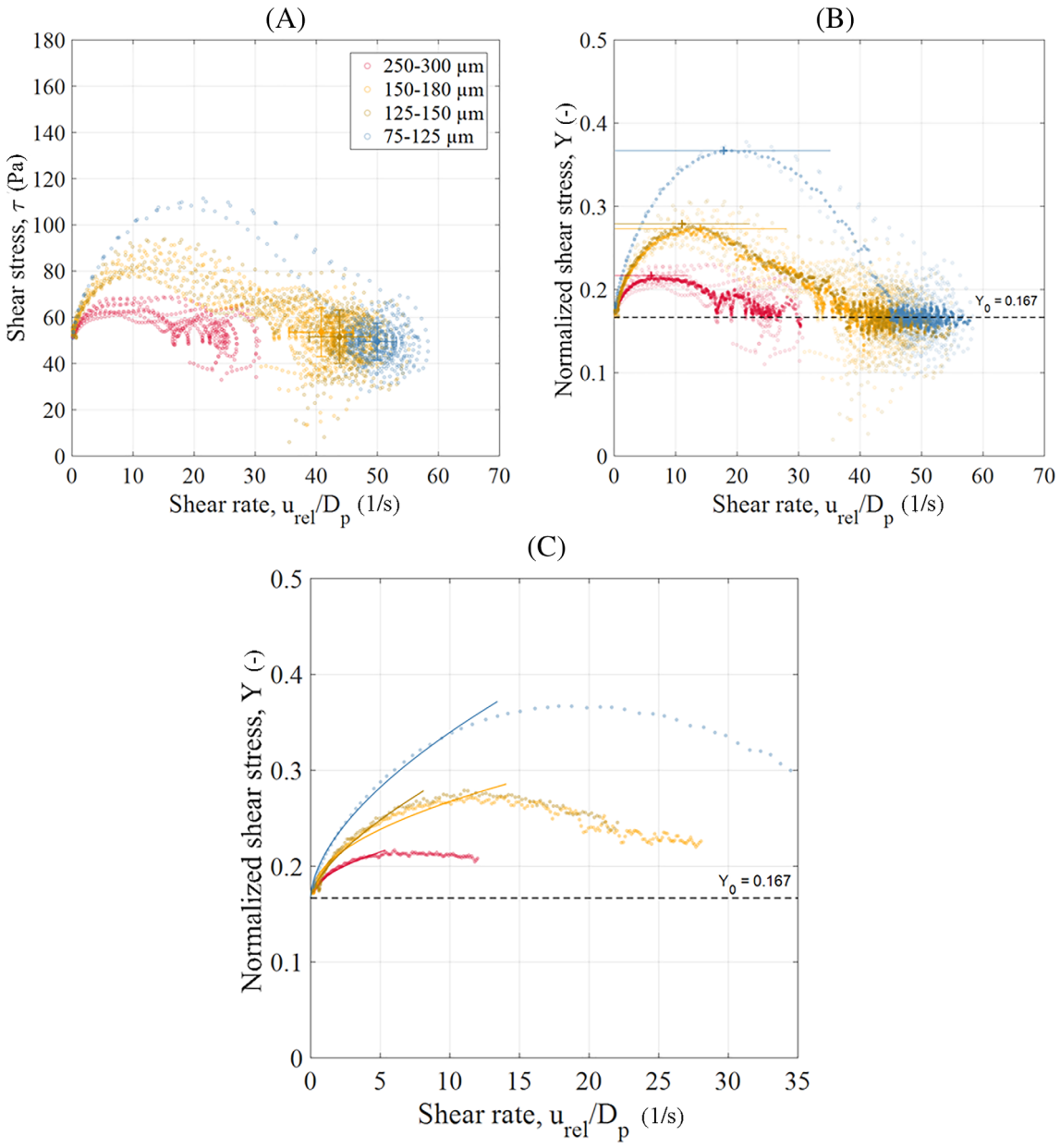

FIGURE 5 Rheograms corresponding to a tracer (here, $T10_4$) during a stagnating trajectory in different bulk materials (here, glass beads of different mean sizes). (A) Absolute variables. The centre of mass (average values) is indicated with a diamond symbol (♦). (B) Normalized variables. The maximum normalized shear stress is indicated with a plus sign (+), and the normalized yield gravity parameter is indicated with a dashed line. (C) Filtered normalized shear stress versus shear rate. Fitting to Equations (8) and (9) is indicated as curves.

and resolve the trajectory of the spherical magnetic tracers, as they rose or sank inside the bed. The porous air distributor plate was designed to ensure a sufficiently high pressure drop to yield a homogeneous spatial and temporal distribution of the air flow, which together with the small cross-section of the bed contributes to enable stable operation under minimum fluidization conditions.

The mass of bulk solids was selected to achieve a height of about 17–18 cm at minimum fluidization, which matched the volume optimized for the tracking method. Depending on the tracer density in relation to the emulsion density, the tracers would either sink or rise (as presented in Table 1), and the experimental procedure was varied as follows.

- For sinking tracers. After an initial test, if the tracer is found to accomplish a steady sinking trajectory in the given bed, the following procedure is used: after vigorous fluidization for a period of 60 s, the fluidization velocity is slowly decreased and set to the corresponding value of u_{mf}. Then, the tracer is held directly above the bed surface and released.

- For rising tracers. Similarly, for tracers that are less dense than the bed, and having first confirmed that the tracer can accomplish a steady ascendant trajectory, the following procedure is used: the tracer is held at the bottom of the container with the help of a thin wire while the bed is fluidized. After 60 s of vigorous fluidization, the fluidization velocity is slowly decreased and set to the corresponding value of u_{mf}. The gas flow is stopped for 2 s to remove the wire, and then restarted to allow the free rising of the tracer.

The absence of bubbles during the tests contributed to the undisturbed, thus, almost perfectly vertical trajectories of the tracers. From visual observations in connection to the injection of the tracer, it was not possible to detect any general impact on the fluidization state of the bed beyond local defluidization in the immediate tracer vicinity (earlier referred to as the de-fluidized hood in literature)[14] or the occasional observation of very small bubbles. The effect of these local phenomena is implicit in the tracer velocity measured and thus accounted for in the calculated effective drag values, as discussed in earlier work.[33] The use of a large bed diameter would have the advantage of reducing the risk of wall effects and minimizing the displacement of the emulsion when the tracer is injected. However, in order to keep the high resolution and accuracy of the tracking system, and because (as explained in Section 2.) the displacement of the emulsion caused by the immersion of the tracer particle was previously found to be negligible (study in the same unit),[33] the current set up is considered to provide the good conditions for the experiments. Note that the short measurement times and the vigorous fluidization previous to each experiment favour the state of homogeneous fluidization for all tests. For each combination of tracer and bulk solids, a minimum of 10 repetitions was carried out. Results regarding statistical robustness are presented in the next section.

3.3 | Identified behaviours

During the experiments, three behaviours were identified that could be used to classify the results. For the sinking trajectories, two behaviours were observed: non-stagnating, for which the tracer sinks all the way down to the air-distributor plate, and stagnating, for which the tracer comes to a stop at some point in the bed. The third behaviour, rising, corresponds to the tracers that are released from the bottom of the bed. In Figure 3, typical velocity profiles for the three behaviours are presented, plotted against the vertical location of the sphere relative to a reference position with a definition specific to each behaviour group (see the left-hand illustration in Figure 3). As exemplified by the data in Figure 3, rising tracers (which start up at the bottom of the bed) exhibit lower velocities during most of their trajectory in the bed compared to sinking tracers, which in turn, after being released, undergo a strong acceleration and then slow down rapidly to zero velocity when stagnating at an intermediate height or when stopping at the bottom of the bed.

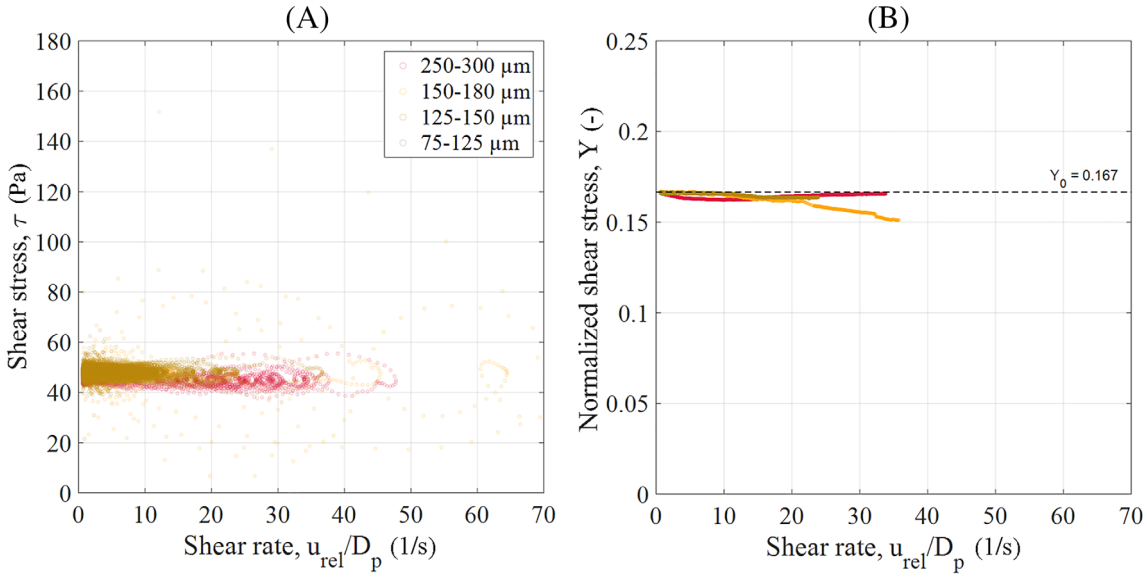

FIGURE 6 Rheograms corresponding to a tracer (here, $T20_9$) during a rising trajectory in different bulk materials (here, glass beads of different mean size). (A) Absolute variables. The centre of mass (average values) is indicated with a diamond symbol (♦) and dashed lines. (B) Normalized variables. The curves are filtered using a moving average. The normalized yield gravity parameter is indicated with a dashed line.

3.4 | Data processing and analysis tools

Tracer trajectories are obtained from the tracking system at a frequency of 200 Hz. These are filtered by applying an 8-point (40 ms) moving average filter to remove noise related to the detection system. The trajectory data are then used to calculate the velocity and acceleration in the vertical direction. As this work studies the drag force imposed on fully immersed particles, the part of the trajectory close to the bed surface is removed from the analysis to ensure full immersion of the tracer and to disregard particle entrance or emersion effects (for sinking and rising behaviours, respectively). For the experiments in which the sphere reaches the bed bottom, the abrupt stop caused by the impact on the distributor plate is also removed. This trajectory cropping is illustrated in Figure 3.

From the cropped trajectory data, the shear stress (u_{rel}/D_p) and shear rate (from Equation (5)) along the tracer trajectory are calculated. By plotting the shear stress (in absolute, τ, and normalized terms, Y) against the shear rates of the three above-described behaviours, some preliminary observations can be made, and the data processing and result analysis applied for each of these behaviours can be described.

- Non-stagnating tracers: The achievement of a constant velocity is evidenced by data-points that are concentrated in a relatively small region (Figure 4A); this is, a narrow range of shear stress and shear rates. Note that

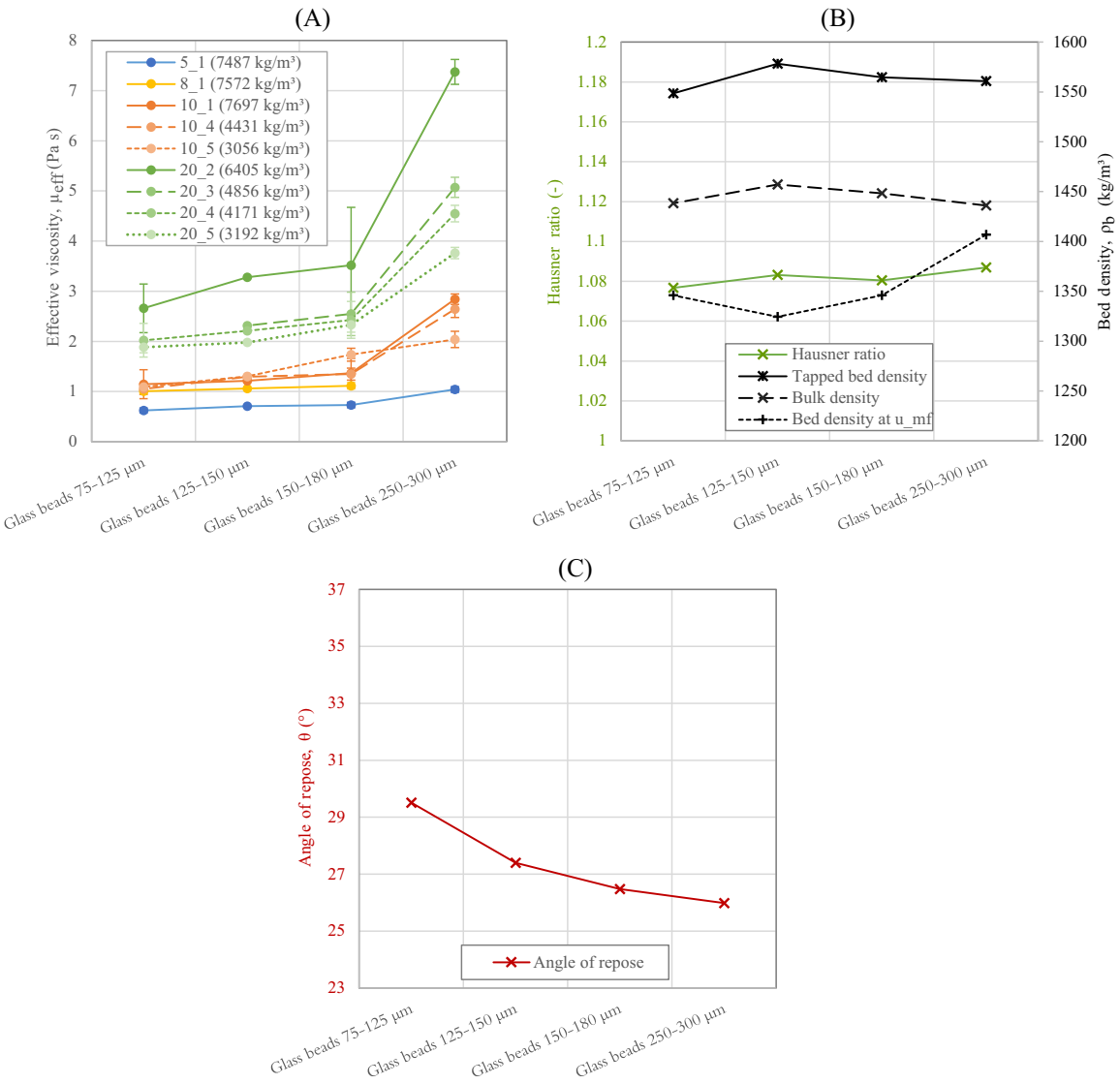

FIGURE 7 Dependence of different parameters on bulk particle size (bulk solids have a particle density of 2486 kg/m^3 and a sphericity of 1). (A) Effective bed viscosity experienced by sinking tracers (as derived from dynamic equilibrium conditions, see Section 3.4). (B) Hausner ratio (left-hand axis) and bulk density (tapped, at rest and at minimum fluidization conditions, right axis). (C) Angle of repose.

these data clouds provide evidence of the achievement of a dynamic equilibrium by exhibiting normalized shear stress values that oscillate around the yield gravity parameter, $Y_0 = 0.167$, in other words, balancing the drag forces with the net gravitational forces (Figure 4B). This type of behaviour is analyzed by calculating the centre of mass (average) and standard deviation in both axes of the data cloud. These average values are used to calculate the effective viscosity experienced by the particle (see Equation (7)), with an example indicated by the dashed lines in Figure 4A. A minimum of three repetitions ensures an error of close to 5%, while 10 repetitions often allow for an error of about 3%.

- Stagnating tracers: These are also characterized by initially yielding a somewhat constant sinking velocity but later deaccelerating, so as to stagnate eventually in the bed. The initial dynamic equilibrium produces a cluster of data that oscillates around the maximum shear rate and the yield stress value, as shown in Figure 5A. This dynamic equilibrium is disrupted as the tracer stagnates, appearing in the plot as increases in the shear stress and normalized shear stress ($Y > Y_0$) that end in a static equilibrium at zero velocity (zero shear rate), namely, the yield stress τ_0 or the yield gravity parameter Y_0, respectively. This type of behaviour is analyzed by calculating the centre of mass of the cloud data corresponding to the initial dynamic equilibrium (Figure 5A; i.e., similarly to the previous case) and by calculating the maximum stress reached during stagnation (indicated with a plus sign on the normalized shear stress in Figure 5B). The part of the stagnation curve in Figure 5B that shows a positive second derivative is then fitted to the Herschel–Bulkley model (Equations (8) and (9)) (see example in Figure 5C). For this purpose, the filtered data obtained from each of the tracers exhibiting stagnation in a given bed are collected, and a single fitting is applied in the range of shear rates that lies below the maximum of the normalized shear stress. The model parameters are used for the analysis in Section 4.
- Rising tracers: These tracers exhibit a velocity with gradually amplified fluctuations (as the tracer moves upwards), although it always remains positive (see Figure 3). This results in a fluctuating increase of the shear rate while the values of the shear stress oscillate around the yield stress value (Figure 6A). For such a behaviour, a moving average was applied in order to filter out the fluctuations and reveal the general trend of the normalized shear stress (Figure 6B), which lies just below the yield gravity parameter indicated with a dashed line.

4 | RESULTS AND DISCUSSION

The difference in the motions of the sinking and rising tracers reported in Section 3.4 agrees to some extent with the observations made by Chhabra[7] regarding bubbles rising inside non-Newtonian fluids, which indicates that the ascendant movement occurs following a spiral pattern in which lateral movement has a relevant contribution and that the shear-thinning or shear-thickening is not evident (on the contrary, the drag tends to show a standard Newtonian curve). An imbalance in the non-vertical forces originating from wake shedding the sphere presumably causes the characteristic fluctuating behaviours, but no conclusive analysis has been carried out on the mechanism governing this behaviour. The rheogram curves obtained for rising tracers exhibit the absence of significant shear-thinning or shear-thickening (Figure 7B), and the filtered normalized shear stress curves obtained from experiments with rising tracers remain almost invariable of changes in the bulk solids despite the strongly differing properties of these.

For sinking tracers, the impacts of the physical properties (size, density, and sphericity) of the bulk solids are reported below, considering both non-stagnating and stagnating behaviours (see Figure 4). The effect of variation of the effective viscosity under the conditions of dynamic equilibrium on the bulk solids properties is evaluated and compared to the variation in other properties of the bed material, such as the bed density (tapped, at rest and at minimum fluidization) and the angle of

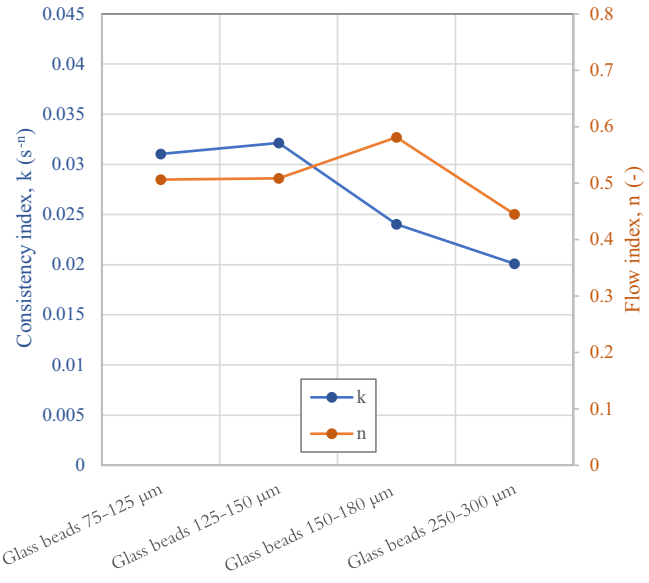

FIGURE 8 Fitted values of the (consistency and flow indices as in Equations (8) and (9)) of the normalized shear stress for beds of different bulk particle sizes.

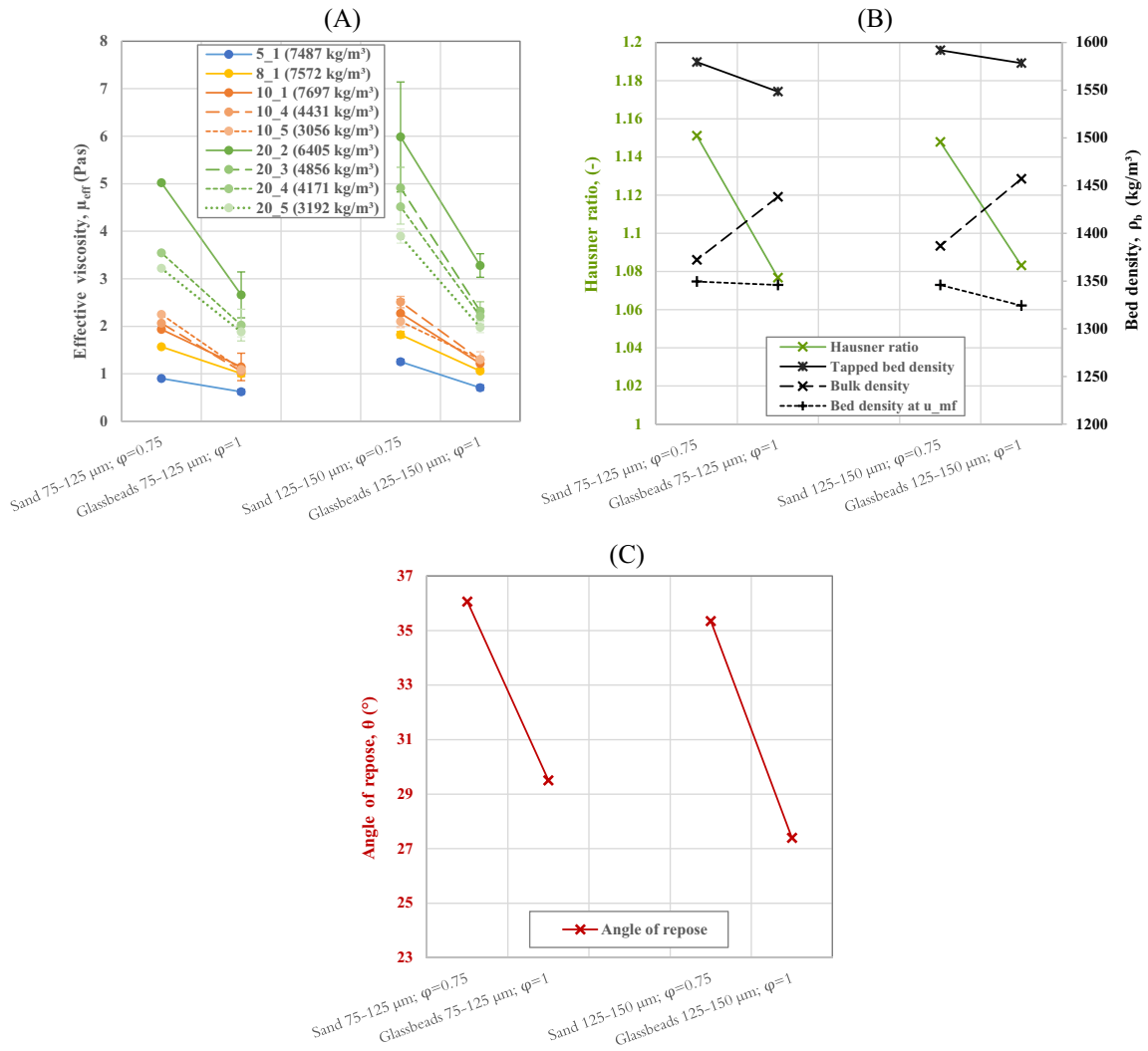

FIGURE 9 Dependence of different parameters on the bulk particle sphericity (sand has a particle density of 2655 kg/m^3 and a sphericity of 0.75). Glass beads have a particle density of 2486 kg/m^3 and a sphericity of 1. (A) Effective viscosity experienced by different tracers sinking in beds with different bulk particle sphericities (as derived from dynamic equilibrium conditions; see Section 3.4). (B) Hausner ratio (left-hand axis) and bulk density (tapped, at rest and under minimum fluidization conditions, right-hand axis). (C) Angle of repose.

repose. Furthermore, the influence of the bed material properties on the drag force at low shear rates is analyzed in terms of the parameters of fitting to the Herschel–Bulkley model (Equations (8) and (9)), that is, the consistency and flow indices.

Regarding the dynamics of the tracer before slowing down to stagnation, it oscillates around an equilibrium velocity (corresponding to the circular pattern in Figure 5A for the finest bed materials) rather than exhibiting a constant velocity. This unstable dynamic equilibrium is at some point broken, and the tracer initiates its path to stagnation. The data do not offer any clear trends in number of oscillations or in the location in the bed that allow for further description of the conditions required for the transition between equilibrium states. Thus, the factors yielding to that of the dynamic equilibrium (i.e., the circular patterns in the rheograms) are broken and tracer stagnation starts are matters for further investigation and are left outside the scope of the present work. Yet, given the high repeatability of the measurements (see Figure 3 as an illustration), the results presented in this work can be considered representative.

4.1 | Effect of bulk solids size

Glass beads in different particle size distribution ranges were used to analyze the effects that the bulk solids size has on the flow characteristics of the bed. Figures 4–6 present typical results obtained from this variation. As exemplified in Figures 4 and 5, smaller bulk solids result in higher shear rates under the conditions of dynamic equilibrium for any given tracer. This yields lower effective viscosities for beds with smaller solids sizes, as

presented in Figure 7A. In addition, the results obtained show consistent quantitative agreement when comparing 5, 8, and 10 mm tracers, which indicates the absence of significant wall effects. However, as explained below, the values for the effective viscosity of the 20 mm tracers may indicate a possible limiting effect of the walls on the rearrangement of the bulk solids.

This higher resistance to movement of an immersed sphere appears to be related to the capacity of the bulk solids to migrate inside the emulsion, as indicated by the bulk properties presented in Figure 7B. As reported by other groups,[14,40,41] a FB with highly confined bulk solids (reflected by a void fraction similar to that at repose) will have more restrictions with respect to the recirculation of the bulk solids and will, therefore, exhibit more inertial effects. This is also reflected in the slightly higher values of the Hausner ratio obtained with increased mean particle size of the bulk solids. Even though the smaller angles of repose measured for larger bulk solids sizes indicate a greater ability of these materials to flow (that is, less cohesion and interlocking among particles and, therefore, an expected smaller resistance to the movement of an immersed body), the weak expansion of the bed from response to minimum fluidization conditions indicates a greater lack of free space in the bed of larger solids, which represents an additional obstacle to the migration of the solids of the emulsion. In turn, this results in a higher resistance to the movement of an immersed object. The smaller the size of the sphere (more similar to the bulk solids size) the less relevant this effect becomes. Moreover, the faster the sphere moves (note that in the same bed, a denser tracer always travels faster due to its higher negatively buoyant force), the more difficult it becomes for the bulk solids to reorganize inside the emulsion, which results in higher effective viscosities.

For stagnating trajectories, the increase in shear stress with shear rate at low shear rates becomes stronger for smaller bulk solids, as presented in Figure 5C. Figure 8 presents the values of k and n (Equation (8)) obtained from fitting the data to the Herschel–Bulkley model. It shows that a bed composed of smaller solids imposes a stronger resistance to the movement of the sphere when the latter approaches a zero-shear rate (zero velocity), that is, the stagnation is more abrupt. However, the flow index appears to be more stable in response to the variation of the bulk solids size. Note that the consistency term follows a trend similar to that exhibited by the angle of repose.

4.2 | Effect of bulk solids sphericity

To explore the effect of bulk solids sphericity, glass beads (rounded solids) were compared with sand (angular solids), with both materials having similar densities. Two different size fractions were tested to confirm the consistency of the results. The results unequivocally indicate higher viscosities for less-rounded bulk solids (Figure 9A). This is in line with the lower bed expansion and higher Hausner ratio detected for the beds with less-rounded solids (Figure 9B). The availability of void space for the bulk particles to move allows the bed to exhibit a lower effective viscosity on a sphere that moves at a relatively high velocity.

The results obtained for the stagnating trajectories are shown in Figure 10. For a given solids size, the consistency index is lower for a bed of sand than for a bed of glass beads. This means that the stagnation within the glass beads occurs with a sharper decrease in the shear rate than it does for the sand. The angle of repose for sand particles is notably higher than for glass beads. Thus, the apparent higher degree of interlocking and possibly more intense friction effects exhibited in sand at repose do not seem to result in a higher viscosity of the emulsion when the tracer approaches zero velocity. The flow index shows a tendency to increase when the sphericity of the bulk particles decreases, which is in line with the higher values for the angle of repose reported for sand particles.

4.3 | Effect of the bulk solids density

For the comparison of the beds with different bulk solids densities, equivalent tracers were selected, namely, tracers with similar buoyant densities. The effective viscosity values calculated based on the conditions of dynamic

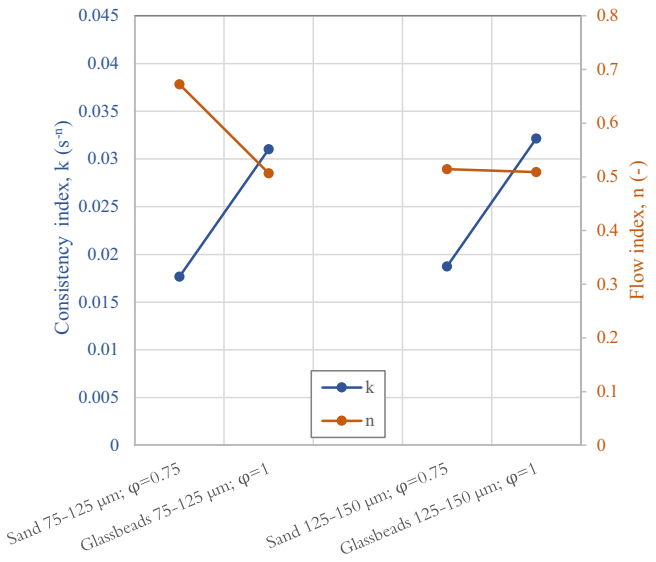

FIGURE 10 Fitted values of the (consistency and flow indices as in Equations (8) and (9)) of the normalized shear stress for beds of different bulk solids particle sphericity.

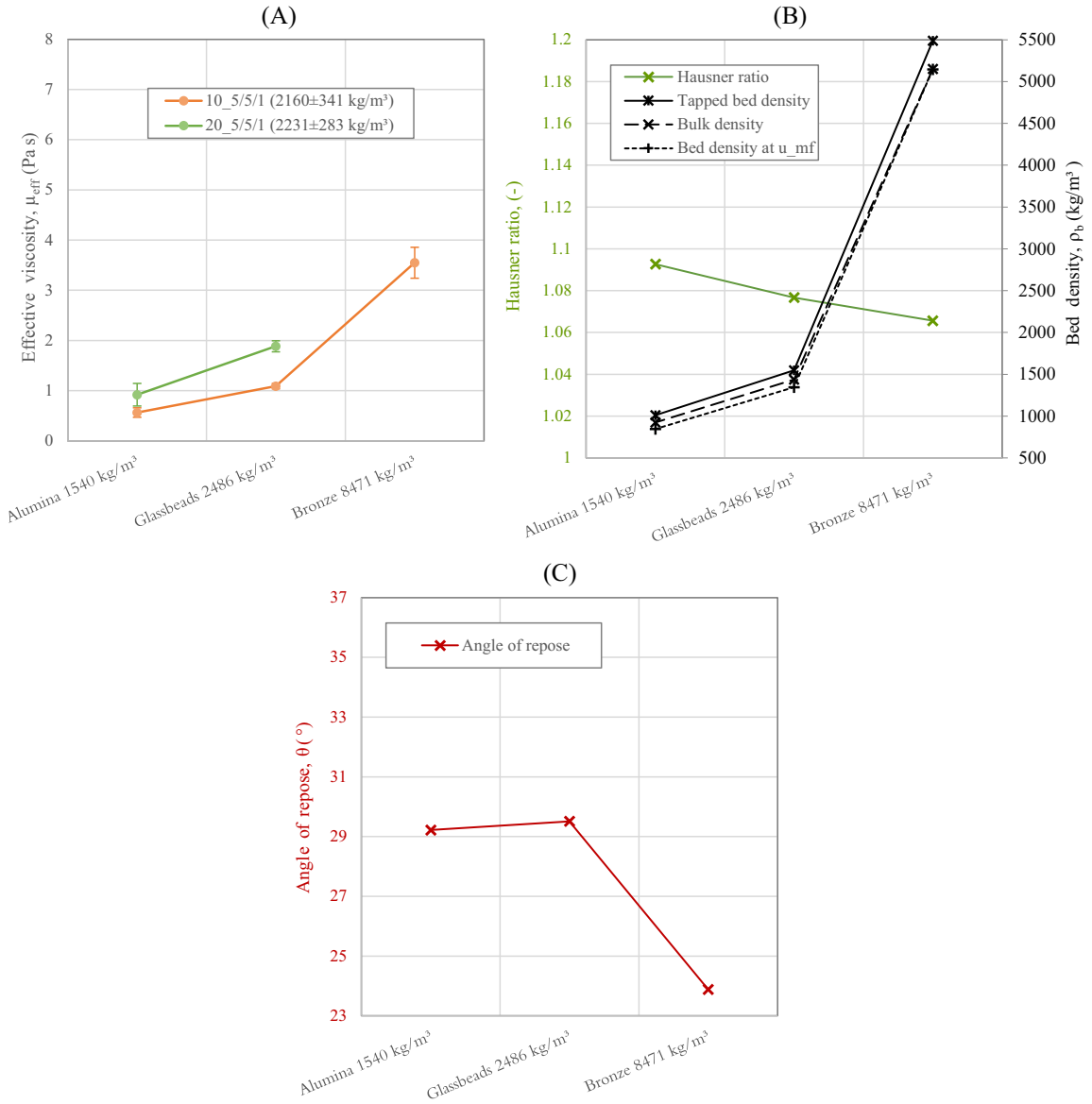

FIGURE 11 Dependence of different parameters on the bulk particle density (all three different bulk solids have particle sizes in the range of 75–125 μm and a sphericity that is close to 1). (A) Effective viscosity experienced by a tracer of 10 mm and a tracer of 20 mm while sinking in beds of different bulk particle densities (as derived from dynamic equilibrium conditions, see Section 3.4). (B) Hausner ratio (left-hand axis) and bulk density (tapped, at rest and under minimum fluidization conditions, right-hand axis). (C) Angle of repose.

equilibrium are presented in Figure 11A. Increases in the density of the bulk solids result in higher effective viscosities. Denser bulk solids exert a stronger resistance towards the movement of the sphere as it enters the bed, which is related to the higher inertia of the denser solids, as well as to the reduced void space available for the solids to migrate as the sphere sinks (note the weaker expansion of the bed from the fixed to minimum fluidization state, and the lower Hausner ratio).

For the stagnating behaviour, only tracers of 10 mm in diameter could be compared among the beds with different bulk solids densities ($T10_1$ for the bed of bronze particles and $T10_5$ for the beds of glass beads and alumina particles). As shown in Figure 12, denser bulk solids yield lower values for the consistency and flow indexes (especially the latter). While the decrease in the consistency index is not very significant, the decrease in the flow index is particularly interesting, as it was scarcely influenced by the size and sphericity of the bulk solids. The flow index correlates with the difference between the bed density at minimum fluidization and at rest, the Hausner ratio, and the angle of repose. Thus, the rate at which this resistance imposed by the emulsion to the movement of a sinking object decreases faster with increases in the shear rate, as the bulk solids grow in density.

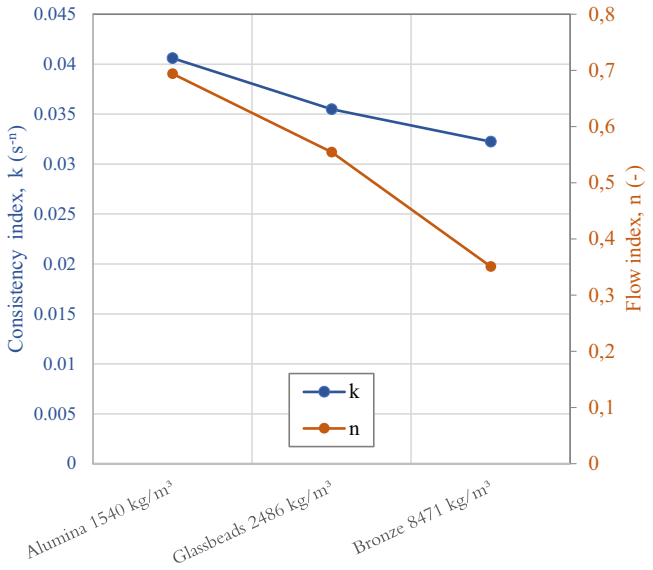

FIGURE 12 Fitted values of the (consistency and flow indices as in Equations (8) and (9)) of the normalized shear stress for beds of different bulk solids density.

5 | CONCLUSIONS

More than 50 years after the pioneering work of Professor J. R. Grace, which proposed to assign a viscosity to the FB, we have used a state-of-the-art magnetic particle tracking system to investigate the influences of bulk solids size, sphericity, and density of Geldart group B solids on the momentum exchange between a dense gas–solids suspension and immersed larger spherical tracers. The details of the tracer-bed momentum transfer for cases with different tracers and bed materials are discussed with the help of rheograms, and the results from the different cases are characterized by an effective viscosity governing the momentum transfer under dynamic equilibrium conditions. Values of this effective viscosity characterizing this momentum transfer are derived from resolved analysis of the shear stress exerted on the tracer at different slip velocities. The shear stress for all the experiments, especially for the case of rising tracers, is characterized by a strong yield stress and a moderate contribution from the shear stress that originates from the shear rate.

In the case of rising spheres, the normalized shear stress was found to be slightly lower than the yield gravity parameter, regardless of the shear rate or the properties of the bulk solids. This strongly non-Newtonian behaviour of the drag from the bed at minimum fluidization is also observed for sinking tracers, which exhibit non-monotonic dependencies between the shear stress and shear rate. This yields two equilibrium states for a given tracer, an unstable equilibrium fluctuating around a falling terminal velocity and a stable equilibrium represented by the stagnation of the falling sphere in the bed.

Higher values of the bulk particle size and density, as well as lower values for the sphericity, are found to increase the effective viscosity of the bed on the sphere at high shear rates. These observations relate to the lower bed expansion and, thus, the consequent stronger restriction on the migration of bulk particles in the emulsion. The Hausner ratio is found to represent a suitable parameter for the qualitative characterization of bulk material in terms of drag on larger spheres, as it consistently provides qualitative trends opposite to the measured values of the effective viscosity.

The relationship between shear stress and shear rate at velocities close to zero (sphere stagnation) shows visco-plastic behaviour, regardless of the properties of the bulk solids. Smaller, more rounded, and lighter bulk solids make up the emulsions that yield higher levels of shear stress. Still, the emulsion thins more slowly with the increase in shear rate for denser and more-rounded particles, which correlates to a certain extent with the lower angle of repose. Thus, greater flowability of the bulk solids in repose is an indication of a faster thinning of the fluidized emulsion. Data from different beds and tracers were, therefore, fitted to the Herschel–Bulkley model, yielding values for the consistency and flow indices.

NOMENCLATURE

Symbols

A_b	cross-sectional area of the bed container (m^2)
A_s	superficial area of the tracer sphere (m^2)
C_D	drag coefficient (−)
D_p	diameter of the tracer sphere (m)
D_b	diameter of the bed container (m)
F_B	buoyancy force (N)
F_D	drag force (N)
F_G	gravity force (N)
F_V	virtual mass force (N)
g	gravitational acceleration (m/s^2)
k	consistency index in the Herschel–Bulkley model (1/s)
k_0	consistency index in the Herschel–Bulkley model for normalized shear stress (1/s)
L_{mf}	height of the bed under minimum fluidization conditions (m)
m_b	mass of the bed (kg)
m_p	mass of the trace sphere (kg)
n	flow-index in the Herschel–Bulkley model (−)
n_0	flow-index in the Herschel–Bulkley model for normalized shear stress (−)
t	time (s)
u_{em}	velocity of the emulsion (m/s)
u_z	vertical velocity of the tracer sphere (m/s)
u_{mf}	minimum fluidization velocity (m/s)

u_{rel} relative velocity of the tracer to the bulk solids velocity (m/s)
Y normalized shear stress (−)
Y_0 yield gravity parameter in the Herschel–Bulkley model (−)

Greek letters

ρ_p density of the tracer sphere (kg/m^3)
ρ_g density of the gas (kg/m^3)
ρ_s density of the bed solids (kg/m^3)
ρ_{em} density of the emulsion (kg/m^3)
ε_{mf} voidage of the bed at minimum fluidization (−)
$\dot{\gamma}$ shear rate (1/s)
φ particle sphericity (−)
λ ratio of sphere velocity to emulsion velocity (−)
τ shear stress (Pa)
τ_0 yield stress (Pa)
μ_{eff} efficient viscosity (Pa s)

AUTHOR CONTRIBUTIONS

Diana Carolina Guío-Pérez: Conceptualization; formal analysis; investigation; methodology; writing – original draft. **Anna Köhler:** Conceptualization; formal analysis; investigation; methodology; writing – review and editing. **Anna Prati:** Investigation; software; writing – review and editing. **David Pallarès:** Conceptualization; funding acquisition; project administration; supervision; writing – review and editing. **Filip Johnsson:** Funding acquisition; supervision; writing – review and editing.

ACKNOWLEDGEMENTS

The research leading to this work was financed by the Swedish Gasification Centre (SFC) within the framework of the Centre for Indirect Gasification of Biomass (CIGB) and by the Swedish Energy Agency within the framework of project P-38347-2.

PEER REVIEW

The peer review history for this article is available at https://publons.com/publon/10.1002/cjce.24575.

DATA AVAILABILITY STATEMENT

Data available on request from the authors

ORCID

Diana Carolina Guío-Pérez https://orcid.org/0000-0001-6415-1148
Anna Köhler https://orcid.org/0000-0002-4484-944X
David Pallarès https://orcid.org/0000-0002-1574-4075
Filip Johnsson https://orcid.org/0000-0003-3106-5379

REFERENCES

[1] P. N. Rowe, A. W. Nienow, *Powder Technol.* **1976**, *15*(2), 141.
[2] E. Sette, T. Berdugo Vilches, D. Pallarès, F. Johnsson, *Appl. Energy* **2016**, *163*, 304.
[3] J. R. Grace, *Can. J. Chem. Eng.* **1970**, *48*, 30.
[4] R. D. Toomey, H. F. Johnstone, *Chem. Eng. Prog.* **1952**, *48*, 220.
[5] J. R. Grace, R. Clift, *Chem. Eng. Sci.* **1974**, *29*(2), 327.
[6] P. N. Rowe, B. Partridge, A. Cheney, G. Henwood, E. Lyall, *Trans. Inst. Chem. Eng.* **1965**, *43*, 271.
[7] R. P. Chhabra, *Bubbles, Drops, and Particles in Non-Newtonian Fluids*, CRC Press, Boca Raton, FL **2007**. https://doi.org/10.1201/9781420015386
[8] A. C. Rees, J. F. Davidson, J. S. Dennis, A. N. Hayhurst, *Chem. Eng. Sci.* **2005**, *60*(4), 1143.
[9] T. C. Daniels, *Journal of Mechanical Engineering Science* **1962**, *4*(2), 103.
[10] T. C. Daniels, *Rheol. Acta* **1965**, *4*(3), 192.
[11] D. F. King, F. R. G. Mitchell, D. Harrison, *Powder Technol.* **1981**, *28*(1), 55.
[12] T. Kai, M. Murakami, K. I. Yamasaki, T. Takahashi, *J. Chem. Eng. Jpn.* **1991**, *24*(4), 494.
[13] L. G. Gibilaro, K. Gallucci, R. Di Felice, P. Pagliai, *Chem. Eng. Sci.* **2007**, *62*(1–2), 294.
[14] A. C. Rees, J. F. Davidson, J. S. Dennis, A. N. Hayhurst, *Chem. Eng. Res. Des.* **2007**, *85*(10), 1341.
[15] K. Schügerl, M. Merz, F. Fetting, *Chem. Eng. Sci.* **1961**, *5*(1–2), 1.
[16] G. Van Den Langenberg-Schenk, K. Rietema, *Powder Technol.* **1984**, *38*(1), 23.
[17] P. Anjaneyulu, D. V. Khakhar, *Powder Technol.* **1995**, *83*(1), 29.
[18] A. Colafigli, L. Mazzei, P. Lettieri, L. Gibilaro, *Chem. Eng. Sci.* **2009**, *64*(1), 144.
[19] S. Chen, R. Cai, Y. Zhang, H. Yang, H. Zhang, J. Lyu, *Powder Technol.* **2021**, *377*, 289.
[20] M. Poletto, D. Joseph, *J. Rheol.* **1995**, *39*(2), 323.
[21] R. Di Felice, P. U. Foscolo, L. G. Gibilaro, S. Rapagna, *Chem. Eng. Sci.* **1991**, *46*(7), 1873.
[22] R. Di Felice, P. Pagliai, *Int. J. Multiphase Flow* **2007**, *33*(7), 797.
[23] M. R. Kamal, A. Mutel, *J. Polym. Eng.* **1985**, *5*(4), 293.
[24] P. Coussot, *Rheometry of Pastes, Suspensions, and Granular Materials: Applications in Industry and Environment*, John Wiley & Sons Inc., Hoboken, NJ **2005**. https://doi.org/10.1002/0471720577
[25] N. Willenbacher, K. Georgieva, *Product Design and Engineering: Formulation of Gels and Pastes*, Wiley-VCH Verlag GmbH & Co., Weinheim, Germany **2013**. https://doi.org/10.1002/9783527654741
[26] G. D. R. MiDi, *Eur. Phys. J. E: Soft Matter Biol. Phys.* **2004**, *14*, 341.
[27] H. de Cagny, A. Fall, M. Denn, D. Bonn, *J. Rheol.* **2015**, *59*, 957.
[28] K. Wu, V. Francia, M. O. Coppens, *Powder Technol.* **2020**, *365*, 172.
[29] T. C. Daniels, *Rheology of Disperse Systems* **1959**, *5*, 211.
[30] J. Li, C. Cheng, Z. Zhang, J. Yuan, A. Nemet, F. Fett, *Chem. Eng. Sci.* **1999**, *54*(22), 5409.
[31] M. Shah, R. Utikar, M. Tade, G. Evans, V. Pareek, *Chem. Eng. Sci.* **2013**, *102*, 365.
[32] E. Sette, D. Pallarès, F. Johnsson, F. Ahrentorp, A. Ericsson, C. Johansson, *Fuel Process. Technol.* **2015**, *138*, 368.
[33] A. Köhler, D. C. Guío-Pérez, A. Prati, M. Larcher, D. Pallarès, *Powder Technol.* **2021**, *393*, 510.
[34] W. H. Herschel, R. Bulkley, *Kolloid-Z.* **1926**, *39*(4), 291.
[35] D. Geldart, *Powder Technol.* **1973**, *7*, 285.

[36] T. R. Auton, J. C. R. Hunt, M. Prud'Homme, *J. Fluid Mech.* **1988**, *197*, 241.
[37] T. Z. Harmathy, *AIChE J.* **1960**, *6*(2), 281.
[38] J. R. Grace, X. Bi, N. Ellis, *Essentials of Fluidization Technology*, Wiley-VCH, Weinheim, Germany **2020**. https://doi.org/10.1002/9783527699483
[39] A. Köhler, D. Pallarès, F. Johnsson, *Fuel Process. Technol.* **2017**, *162*, 147.
[40] P. T. Reardon, A. L. Graham, S. Feng, V. Chawla, R. S. Admuthe, L. A. Mondy, *Rheol. Acta* **2007**, *46*, 413.
[41] L. A. Mondy, C. Retallack, K. Thompson, J. Barney, A. Grillet, A. L. Graham, *AIChE J.* **2008**, *54*(4), 862.

How to cite this article:
D. C. Guío-Pérez, A. Köhler, A. Prati, D. Pallarès, F. Johnsson, *Can. J. Chem. Eng.* **2022**, 1. https://doi.org/10.1002/cjce.24575